Available online at www.sciencedirect.com
ScienceDirect
Tectonophysics 447 (2008) 5 – 18
TECTONOPHYSICS
www.elsevier.com/locate/tecto

The effect of the large-scale mantle flow field on the Iceland hotspot track

Peter Mihalffy [a,*], Bernhard Steinberger [b], Harro Schmeling [a]

[a] J.W. Goethe-University 60323 Frankfurt M, Germany
[b] Center for Geodynamics, NGU, 7491 Trondheim, Norway

Received 27 September 2005; received in revised form 4 April 2006; accepted 4 December 2006

Abstract

Fluid dynamical simulations were carried out in order to investigate the effect of the large-scale mantle flow field and the depth of the plume source on the structure of the Iceland plume through time. The time-dependent location and shape of the plume in the Earth's mantle was calculated in a global model and it was refined in the upper mantle using a 3D Cartesian model box. Global flow was computed based on density heterogeneities derived from seismic tomography. Plate motion history served as a velocity boundary condition in both models. Hotspot tracks of the plume conduits and the plume head were calculated and compared to actual bathymetry of the North Atlantic. If a plume source in the lowermost mantle is assumed, the calculated surface position of the plume conduit has a southward component of motion due to southward flow in the lower mantle. Depending on tomography model, assumed plume age and buoyancy the southward component is more or less dominating. Plume models having a source at the 660 km discontinuity are only influenced by flow in the upper mantle and transition zone and hence rather yield westward hotspot motion. Many whole-mantle plume models result in a V-shaped track, which does not match the straight Greenland–Iceland–Faroe ridge. Models without strong southward motion, such as for a plume source at 660 km depth, match actual bathymetry better. Plume tracks were calculated from both plume conduits and plume heads. A plume head of 120 K anomalous temperature gives the best match between plume head track and bathymetry.

Keywords: Plume–ridge interaction; Mantle flow field; Tilted plume; Hotspot track; Upper-mantle plume

1. Introduction

1.1. Plume hypothesis

Two of the major outstanding problems in mantle convection are the origin of plumes and their relation to mid-oceanic ridges. While the classical plume hypothesis (Morgan, 1971) and the majority of subsequent studies postulate the origin of plumes to be related to a thermal boundary layer at the core mantle boundary, this view has been questioned recently (Anderson, 2000). Davaille (1999) showed in laboratory experiments a doming regime of thermo-compositional convection combined with narrow hot thermal plumes rising from the top of the domes. Courtillot et al. (2003) suggest various depths of origin for different plumes, as also seen in finite frequency seismic tomography studies (Montelli et al., 2004). In particular the depth of origin of the Iceland plume has been debated controversially: While Bijwaard and Spakman (1999) present clear seismological evidence for a deep origin, Montelli et al., (2004) loose the plume related tomography signal between 1000 and 2000 km depth, and Foulger et al. (2000) argued that the seismic anomaly below Iceland extends to the transition zone and not deeper. Given these alternative views dynamic models of a mantle plume interacting with the large-scale mantle flow field might help to resolve the question.

Originally, the plume hypothesis was postulated to explain the existence of the island chains of the Pacific by a strong hot upwelling mantle flow (Morgan, 1971) relative to which the lithosphere moves. However, plumes may also interact with, or be captured by spreading ridges (Ito et al., 2003; Jellinek et al., 2003). In a time-dependent ridge-feeding model for the North Atlantic (Vink, 1984) a fixed Iceland plume has transported material to the closest part of the migrating mid-Atlantic ridge.

* Corresponding author.
E-mail address: mihalffy@geophysik.uni-frankfurt.de (P. Mihalffy).

0040-1951/$ - see front matter © 2007 Elsevier B.V. All rights reserved.
doi:10.1016/j.tecto.2006.12.012

This model succeeded to predict the orientation and age progression of the Faroe-Greenland and the Vøring plateaus, assuming an interaction radius of at least 700 km. The lithospheric thickness increases away from ridges due to lithospheric cooling. This forms a negative drainage pattern for buoyant material under the lithosphere, which could be of importance for controlling plume head motion (Kincaid et al., 1996). Ribe and Delattre (1998) find that interaction of plume and ridge is stronger when they move away from each other than towards each other.

1.2. Geophysical indication of the Iceland plume

Location of the Bouguer anomaly minimum and the thickest crust from receiver function analysis (Thorbergsson et al., 1993; Shen et al., 2002) indicate a present-day location of the Iceland plume at 18° W, 64.4° N. The crust of Iceland and the aseismic Faroe–Iceland ridge (Fig. 1) has been extensively studied by seismic methods (Menke and Levin, 1994; Staples et al., 1997; Brandsdottir et al., 1997, Smallwood, 1999).

The FIRE experiment (Faroe–Iceland Ridge Experiment; Staples et al., 1997) has investigated the crust and the upper mantle along the aseismic Faroe–Iceland Ridge between Faroe Islands and the present-day spreading center. They found that the crust along the Faroe–Iceland ridge is 25–30 km thick (Smallwood, 1999), which indicates, that the mantle potential temperature is elevated by 200–250° C above normal. Similar crustal thickness (25–35 km) has been inferred for the Greenland–Iceland ridge (Fig. 1) from crustal isostacy studies by Kaban et al. (2002). Under the Northern Volcanic Zone of Iceland the FIRE experiment constrained a crust of 19 km and at the older Tertiary areas of north-eastern Iceland a 35 km thick crust. The pronounced thickened crust of the Greenland–Iceland–Faroe ridge is suspected to be a geologic record of the interaction of the mid-Atlantic ridge with the Iceland plume (White, 1997). Using locally-recorded earthquake data Menke and Levin (1994) have investigated the crustal structure of central Iceland. The experiment shows a crustal thickness of 22 km. As the Iceland plume might have affected the region north of present-day Iceland, it is of interest to assess crustal thickness anomalies in this region. While the crust around the Kolbeinsey ridge (Fig. 1) has almost normal oceanic thickness (Kodaira et al., 1997), the aseismic south Jan Mayen ridge (Fig. 1) between Iceland and Jan Mayen has an anomalous crust of 20 km (Evans and Sacks, 1979), and is generally regarded as a continental fragment. Here, the total lithospheric thickness is 50 km, which compensates isostatically the thick crust (Evans and Sacks, 1979). On the mid-Norwegian passive margin the oceanic crust in the southern area is thicker than in the northern part, possibly because it was generated by hotter material (Kodaira et al., 1995).

1.3. Mantle flow in the North Atlantic

Given appropriate rheological assumptions, the flow structure of the mantle can be calculated based on density anomalies derived from seismic tomography and surface plate velocities

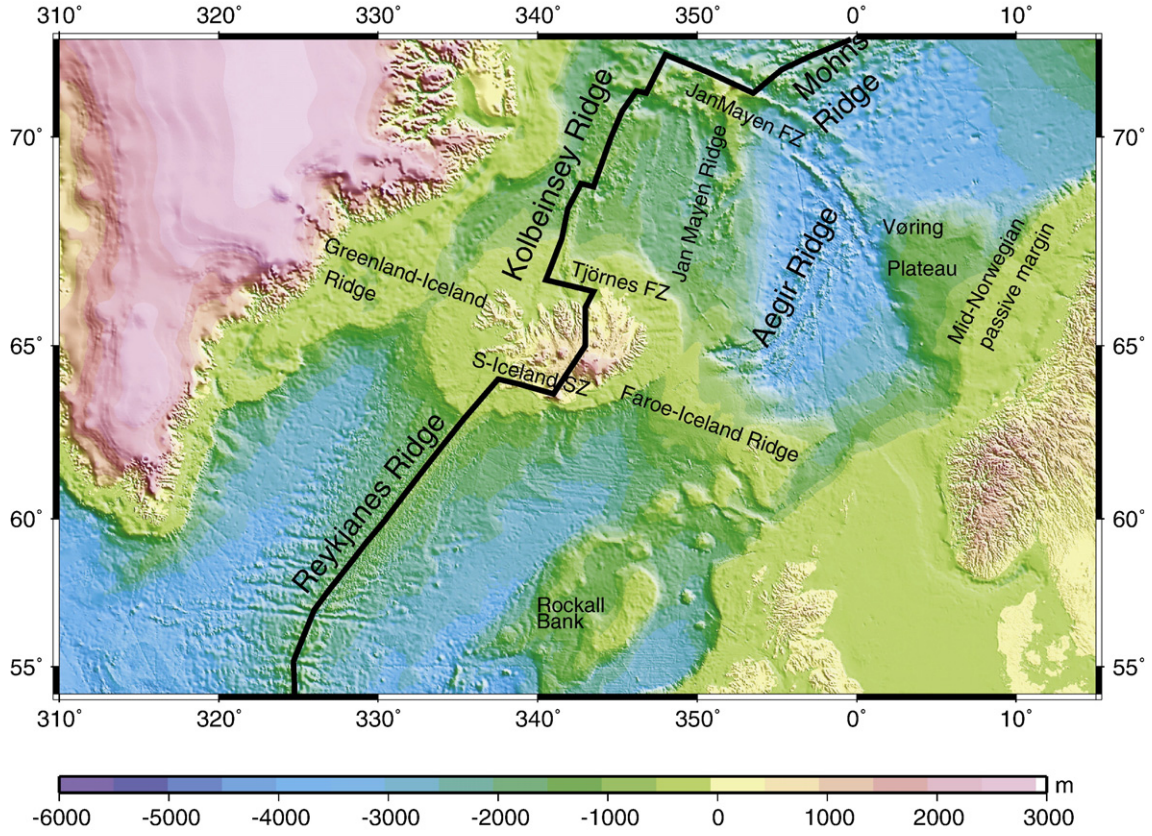

Fig. 1. Bathymetry and ridges in the North Atlantic.

Table 1
Summary of modeling assumptions for flow computations

Model	NR	PM	Age	TM	PRI
1	+	Fixed	–	–	–
2 a	+	D″	60 Ma	smean	–
2 b	+	D″	60 Ma	S20RTS	–
2 c	+	D″	60 Ma	TXBW	–
2 d	+	D″	60 Ma	SB4L18	–
2 e	–	D″	60 Ma	smean	–
2 f	+	D″	80 Ma	smean	–
2 g	+	660	–	smean	–
2 h	+	D″	60 Ma	MK12WM13	–
3 a	+	D″	60 Ma	MK12WM13	+
3 b	+	Fixed	–	MK12WM13	+

Column 1: model number; column 2: NR specifies whether a net rotation of the lithosphere relative to the deep mantle is introduced (+) or not (−); column 3: PM specifies whether the hotspot is assumed fixed, or computed hotspot motion is considered. In the latter case, plume source is either at the top of the D″ layer or depth 660 km. Column 4: age for which (in case of plume source at D″) vertical conduit is assumed. Column 5: TM = tomography model used to compute density heterogeneities: S20RTS (Ritsema and van Heijst, 2000), TXBW (Grand, 2002), SB4L18 (Masters et al., 2000), smean (Becker and Boschi, 2002), or MK12WM13 (Su and Dziewonski, 1997). Column 6: PRI specifies whether plume–ridge interaction is computed in the regional flow model (+) or not (−).

(Hager and O'Connell, 1979, 1981). Data coverage of S wave tomography models in the upper mantle is higher than that of P wave models (Becker and Boschi, 2002). By advection and neglecting thermal diffusion the density anomalies can be predicted also in the past (Steinberger and O'Connell, 1998; Kaus and Podladchikov, 2001; Bunge et al., 2003; Conrad and Gurnis, 2003).

Zhang and Christensen (1993) found that lateral viscosity variations due to temperature dependent rheology do not significantly improve the fit to the gravity potential compared to models using radially varying viscosity only. Cadek and Fleitout (2003) however found that the fit can be improved by including lateral viscosity variations in the top 300 km. These models are long-wavelength approximations, but viscosity variations on the short length scale might be important for plumes. Based on a regional part of a global seismic tomography model, Marquart and Schmeling (2004) have determined the flow structure within the North Atlantic and below Iceland and found best fits to the geoid and gravity for a viscosity jump of not more than a factor of 50 between the upper and lower mantle and a temperature dependent viscosity changing one order of magnitude for 500 K temperature variation. The local direction of the mantle flow can be estimated also from seismic anisotropy analysis (Bjarnason et al., 2002), although near other rift systems anisotropy has been explained also by magma-filled cracks, rather than asthenospheric flow (Gao et al., 1997). Under Iceland a north- or southward flow is expected in the asthenosphere (Bjarnason et al., 2002). Also, it should be noted that the presence of water or melt channels might lead to fast seismic directions which are perpendicular to the flow directions (see: Ruedas and Schmeling, this issue, and references therein).

The experimental and numerical models to date make simplifying assumptions, or are of low resolution, and a direct quantitative comparison of model output with geological and geophysical field observations was so far not possible. Here we therefore present a numerical model of the interaction of Iceland plume and mid-Atlantic ridge that is more actualistic in a number of aspects:

- The model includes global mantle flow, which is computed based on surface plate velocities and mantle density anomalies derived from seismic tomography.
- The model uses detailed time-dependent relative plate motion history and ridge geometry, based on marine magnetic anomalies, and lithospheric thickness variations based on it.
- Location of the plume relative to the ridge is time-dependent and based on global plate reconstructions combined with either fixed or moving-hotspot models.

These aspects are important to quantitatively understand the evolution of the North Atlantic: Distribution of volcanism critically depends on the plume location relative to the ridge; how the plume material distributes in the asthenosphere depends on both large-scale flow and lithospheric thickness variations. We will use a two-fold approach: In a first step (Section 2), the time-dependent location of the Iceland plume is computed with the model of Steinberger et al. (2004). Here the effect of different modeling assumptions on results is tested. In the second step (Section 3), a fully dynamic calculation is performed with an adaption of the model of Albers (2000a,b), in order to achieve a more quantitative treatment of plume–ridge interaction. The calculated distribution of volcanic activity, i.e. the "hotspot track" is compared against the topography of the Greenland–Iceland–Faroe ridge (Smith and Sandwell, 1997; Fig. 1).

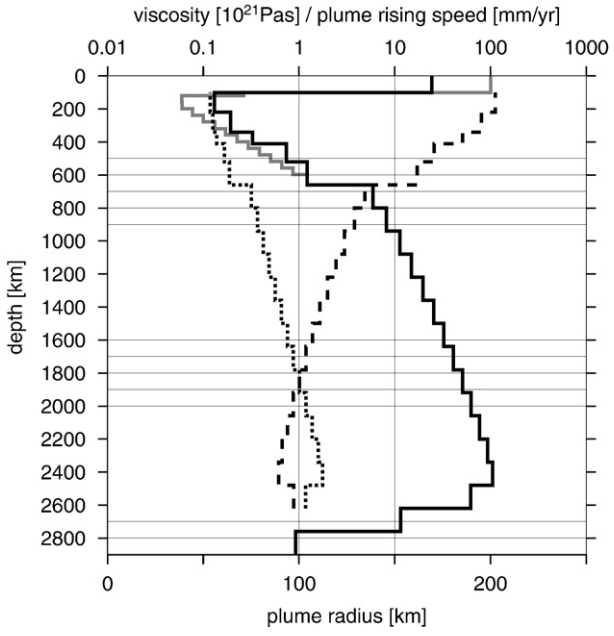

Fig. 2. Assumed profiles of ambient mantle viscosity (upper scale, continuous line, black for models 2 a–g, grey for models 2 h and 3), plume radius (lower scale, dotted line) and buoyant plume rising speed (upper scale, dashed line) vs. depth in the mantle.

2. Iceland plume motion in a global mantle flow model

2.1. Global flow calculation

Computation of a global mantle flow field is required for all except the "fixed hotspot" model case 1 in Table 1) — both without (model cases 2) and with (cases 3) regional flow refinement. Global mantle flow is computed with the method of Hager and O'Connell (1979, 1981). The flow is driven by imposed plate velocities and internal density inhomogeneities derived from seismic tomography. Solving for the conservation of mass and momentum the instantaneous viscous Stokes-flow is calculated. A time-dependent mantle flow field was obtained by backward-advection of mantle density anomalies (Steinberger and O'Connell, 1998) and with time-dependent plate motions.

Tomography models used are shown in Table 1. We use a conversion factor from s-wave speed to density variations $(\delta\rho/\rho)/(\delta v_s/v_s)=0.25$ below 220 km depth, (models 2 a–g in Table 1) or 0.2 (models 2 h and 3) close to what is inferred from mineral physics (Karato, 1993). Variations above 220 km depth are not considered, as they may be caused by compositional variations in the lithosphere.

The mantle viscosity profiles used are shown in Fig. 2. Upper-mantle viscosity in models 2 h and 3 is based on Albers (2000b). Model calculations 2 a–g also considered compressibility and phase boundaries as in Steinberger et al. (2004).

2.2. Plate motions as boundary condition for mantle flow

Plate motions in models 2 h and 3 are from the compilations of Müller et al. (1993) – e.g. motion of North America vs. Africa – and Gordon and Jurdy (1986) – e.g. motion of Greenland and Eurasia vs. North America. In models 2 a–g plate motion "model 2" of Steinberger et al. (2004) was used.

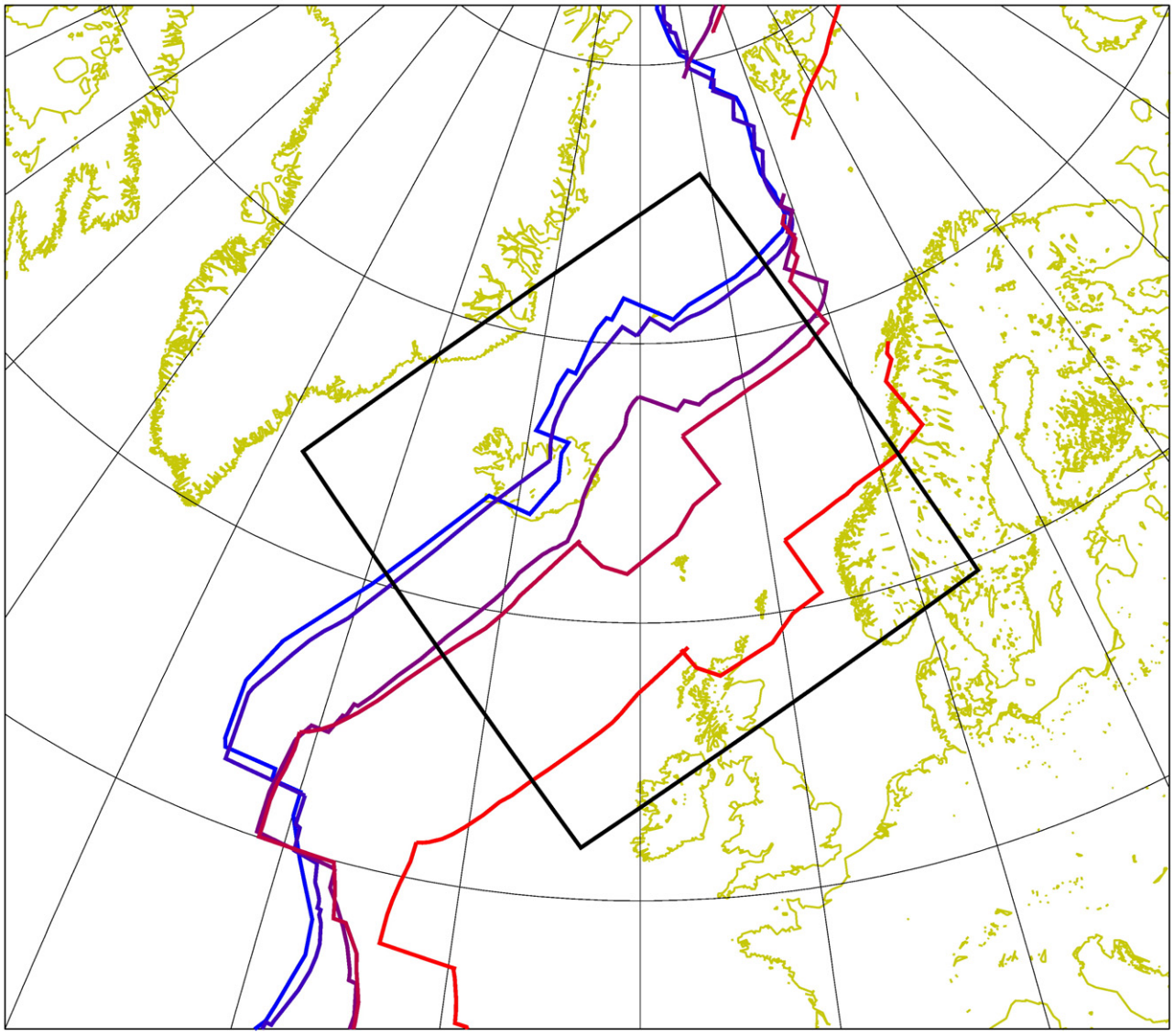

Fig. 3. Plate boundaries interpolated with 2 Ma time interval based on the magnetic anomalies of the ocean floor and the box area of the regional model. Plate boundaries are shown for 0 Ma (blue), 10 Ma, 32 Ma, 34 Ma, 56 Ma (red). The boundaries are getting older towards the southeast in the box area.

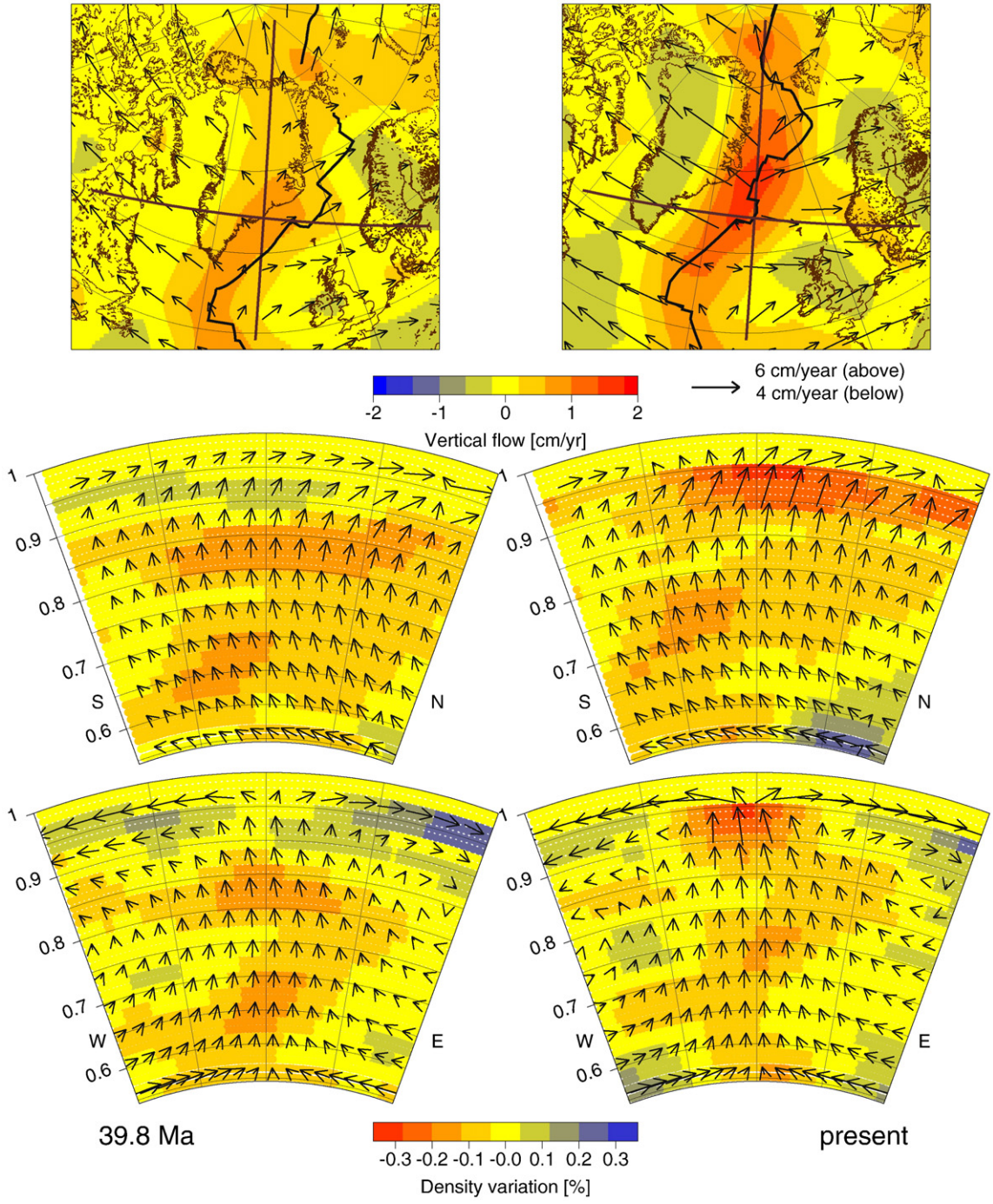

Fig. 4. Flow field in the North Atlantic with the same modeling assumptions as in the moving-source model of Steinberger et al. (2004) and model cases 2 a, f and g in Table 1. Top panels show flow at depth 215 km, second and third row are cross sections through density anomalies and flow along the N–S and E–W profiles indicated in the top panels. Left column for time 39.8 Ma, right column for present-day. Lithosphere motions are in the moving-hotspot reference frame of Steinberger et al. (2004), lower-mantle motions in a no-net-rotation reference frame, with a smooth transition between both frames. For 39.8 Ma, past ridge locations are plotted, and continental outlines rotated in the same mantle reference frame. No density anomalies above 220 km depth are considered for present-day; past density anomalies are computed through backward-advection.

Lithospheric net rotation has been removed in models 2 except for case 2 e; treatment of net rotation in model 3 is explained in Section 3.1.

A global plate boundary model (Gordon and Jurdy, 1986) was used. For model cases 2 h and 3, i.e. including those models with regional flow refinement calculation, it was refined in the Iceland region using magnetic isochrons of Müller et al. (1997) which were rotated to the past ridge position in the hotspot reference frame. Plate boundaries at 2 Ma time intervals were inferred from the isochrons assuming constant geometry and symmetric spreading for given time intervals (Fig. 3). The two major ridge jumps evident in Fig. 3 were introduced between 34 and 32 Ma as

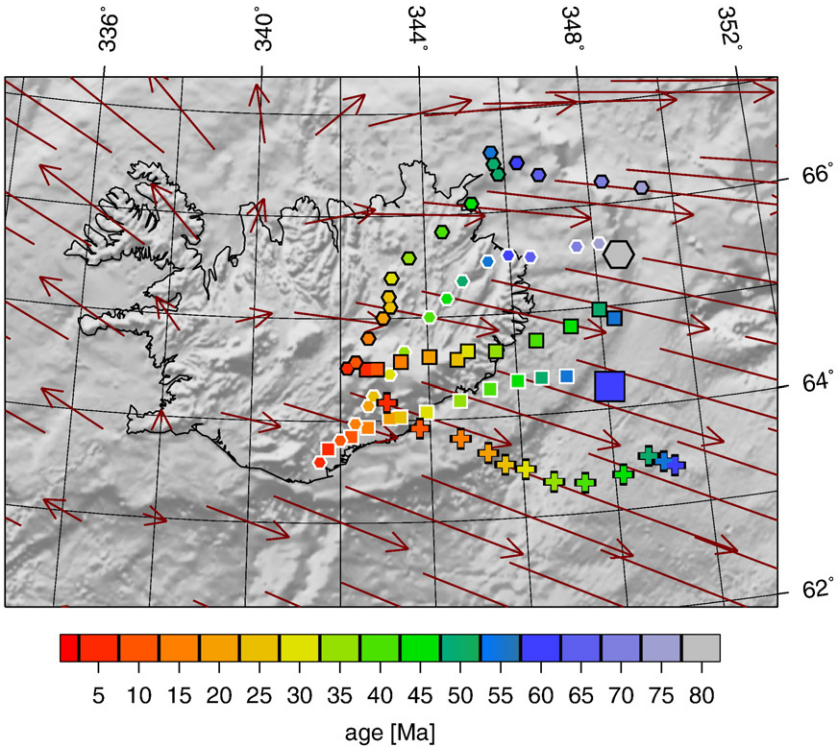

Fig. 5. Plume conduit motion for cases 2 a (squares), f (hexagons) and g (crosses) of Table 1. Plume conduit position at 100 resp. 660 km depth is shown by symbols framed in black resp. white. Conduit position at initial time is shown as big symbols in cases 2 a and f. Iceland coastline is shown for scaling. The shaded relief shows the topography dataset topo_8.2.img from Smith and Sandwell (1997). Arrows show the corresponding asthenospheric present-day flow at depth 215 km; 1° of arc corresponds to 2 cm/yr flow speed.

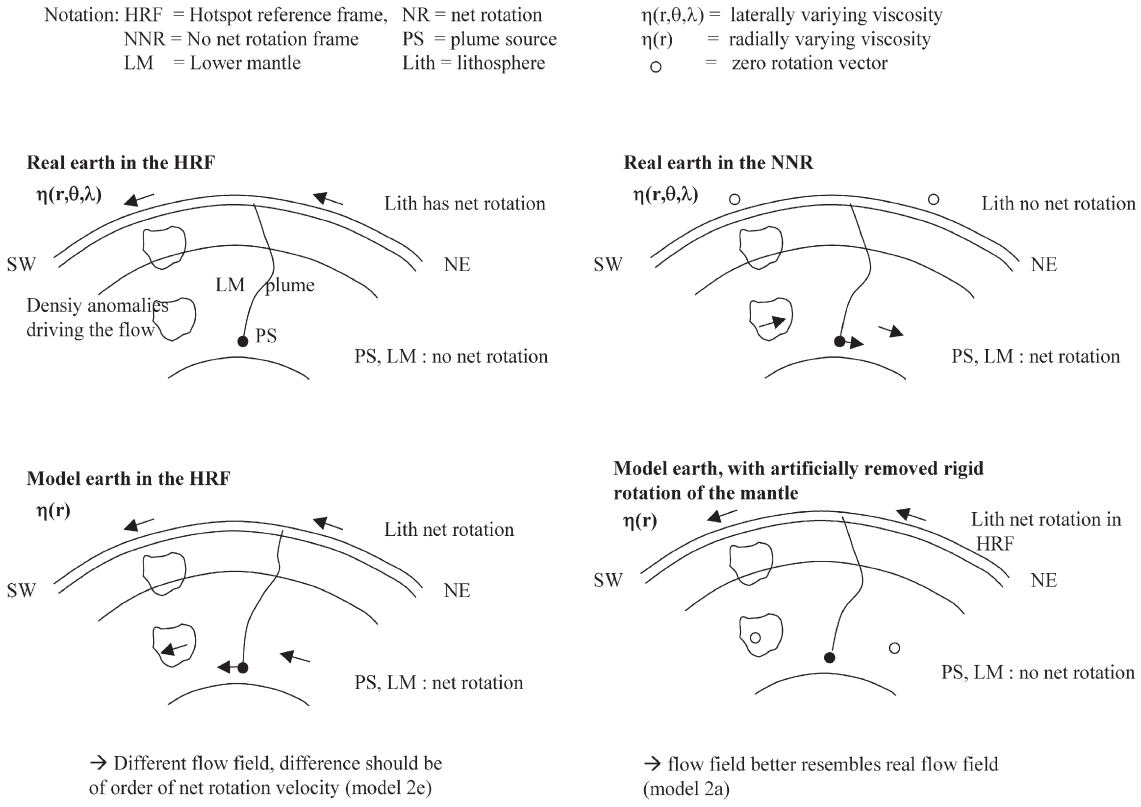

Fig. 6. Schematic sketch showing the different reference frames for earth systems with different rheology assumptions. In systems with purely radially dependent viscosity a net rotation between different shells is physically not possible, while laterally variable viscosity might lead to different net rotations. Approximate directions SW (southwest) and NE (northeast) apply to the region around Iceland.

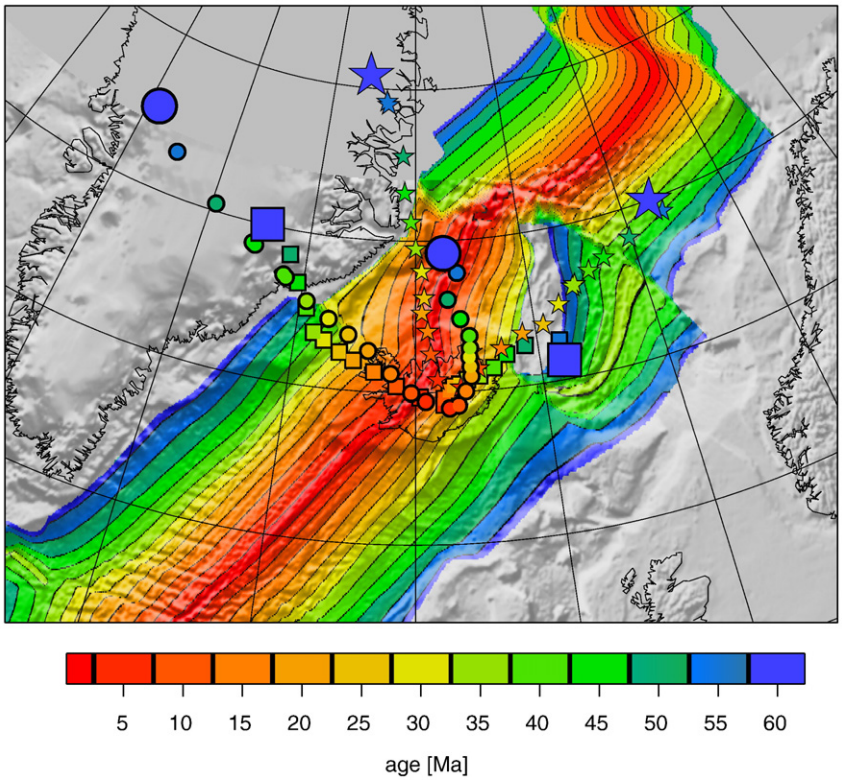

Fig. 7. Hotspot tracks relative to Greenland and Eurasia calculated with different reference frames. Circles are for model 1, squares for model 2 a. Note that the difference between models 1 and 2 a is due to both motion of the Iceland hotspot in model 2 a, and the different absolute plate motion reference frames (Müller et al., 1993 vs. Steinberger et al., 2004). Stars are for model 2 e, i.e. without net rotation of the lithosphere relative to the deep mantle. Big symbols are for initial time 60 Ma. On the same color scale, the seafloor age grid age_1.6 from Muller et al. (1997) is shown. Note that any segment of a computed track cannot correspond to an actual hotspot track if the age is older than the lithosphere age at the same location. Those segments are plotted for the assessment of possible plume–ridge interaction. The shaded relief shows the topography dataset topo_8.2 from Smith and Sandwell (1997).

well as 6 Ma and 4 Ma in the model. The geometry of the oldest available isochron (chron 21) was also used back to 56 Ma, the age of the oldest plate boundary used in the calculation.

2.3. Resulting mantle flow field

The basic flow pattern is characterized by a northward flow in the upper mantle and a southward flow in the lower mantle (Fig. 4). This flow pattern is robust and independent of the tomography model used; it is part of the outward and return flow related to the large-scale upwelling under south Africa. In the upper part of the lower mantle, the horizontal flow component tends to be westward. Due to backward-advection, the Iceland plume at 39.8 Ma is only present in the lower mantle. The regional forward-model of the Iceland plume introduced in the next chapter partly compensates for this shortcoming of the backward-advection procedure.

2.4. Calculation of hotspot motion, hotspot tracks

Advection of a buoyantly rising plume conduit is calculated in the mantle flow field (Steinberger and O'Connell, 1998). Motion of each point along the conduit is computed as the vector sum of large-scale mantle flow and a vertical buoyant rising velocity, which depends on viscosity of the surrounding mantle, hence on depth. Conduit elements enter the lowermost layer and leave the uppermost layer upward. This lowermost "source" layer was usually assumed at depth 2620 km (approximately corresponding to the top of the D″ layer), but a source depth 670 km was considered in model 2 g. In the case of a D″ source, the conduit was assumed vertical at the initial time (usually 60 Ma, except for model 2 f with 80 Ma). For a source depth 670 km, no assumption about an initial conduit is made; instead, all conduit elements are assumed to originate at depth 670 km. Therefore results are independent of an initial time. The starting position of the conduit was chosen in a way to match the present-day "surface" position of the Iceland hotspot at 18° W, 64.4° N in the uppermost layer, assuming the base of the lithosphere at 100 km depth. Other modeling assumptions are described for the "moving-source model" of Steinberger et al. (2004).

Radius and buoyant rising speed of the plume conduit computed with equations given in the supplement to Steinberger et al. (2004) for an anomalous mass flux $1.2 \cdot 103$ kg/s (Sleep, 1990; Schilling, 1991) are shown in Fig. 2. Slightly different model parameters were used for model 2 h.

Corresponding hotspot tracks are computed with a plate motion model that has been slightly modified compared to Section 2.2, in that relative motion of Eurasia vs. North America is adopted from Gaina et al. (2002), Greenland vs. North America from Roest and Srivastava (1989) in model

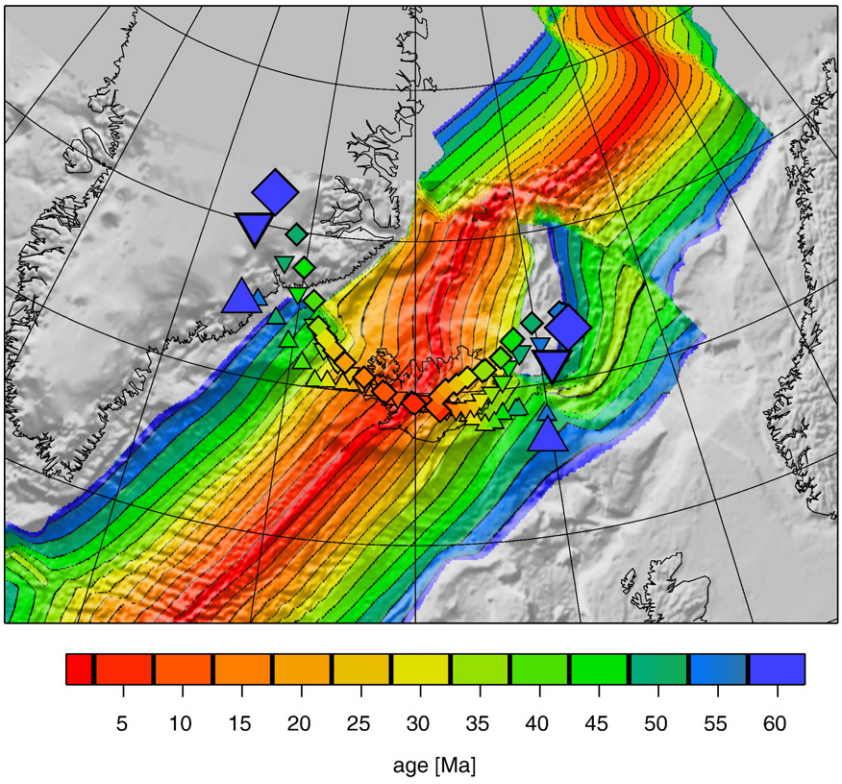

Fig. 8. Hotspot tracks relative to Greenland and Eurasia calculated with different tomography models. Inverted triangles are for model 2 b (S20RTS), diamonds for 2 c (TXBW), triangles for 2 d (SB4L18). Big symbols are for initial time 60 Ma. Different tomography models are used to calculate the motion of the Iceland hotspot, however, the same absolute plate motion model (Steinberger et al., 2004) is maintained in all cases. See Fig. 7 for further explanations.

cases 1 and 2 a–g, and lithospheric net rotation is maintained in all cases.

2.5. Effect of plume age and source depth on resulting conduit motion

The effect of different plume age (cases 2 a vs. f) and source depth (2 a vs. g in Table 1) on the movement of the plume conduit at 660 km and 100 km depth is shown in Fig. 5: Results typically show about 300 km westward motion, but variable amounts of southward motion: Computed plume locations at 60 Ma differ by about 300 km, mainly in N–S direction, among the models shown. The difference of plume position at 100 km and 660 km shows the computed plume tilt in the upper mantle: During the first few Ma after emplacement of an initially vertical conduit, hotspot motion reflects horizontal mantle flow in the upper mantle (cases 2 a and f only). Afterwards, the tilt tends to be approximately steady-state, with the plume location at depth 660 km approximately 100 km further south to southwest than at depth 100 km, and the computed motion of the upper-mantle conduit then tends to represent flow at depth 660 km, if the source of the plume is assumed at that depth, or flow in the upper part of the lower mantle, if a D″ source is assumed. The computed change of hotspot motion direction is therefore a consequence of the mantle flow in different direction at different depths. Hotspot motion tends to represent flow at greater depth for greater plume age or larger plume buoyancy flux. Computed mantle flow beneath Iceland changes from ≈0.5–1 cm/yr west- to northwestward flow at depth 660 km to south- to southwestward flow at similar speed in the lower part of the mantle, and this explains the variation of results. An even larger southward component of motion is computed for even older assumed age, or larger buoyant rising speed. Results for different tomography models vary in a similar manner, and are further discussed below.

Fig. 5 also shows the corresponding present-day asthenospheric flow, computed with the global flow code in a reference frame half-way intermediate between the hotspot and no-net rotation reference frames. This gives a preliminary indication where plume material is transported to in the asthenosphere due to large-scale flow, which is refined in the regional model in Section 3.

2.6. Effect of reference frame choice on resulting hotspot tracks

The computed track position relative to lithosphere of same age formed at the ridge on the same plate indicates relative location of plume and ridge at that time and allows semi-quantitative assessment of plume–ridge interaction. Fig. 7 especially shows the dependence of the computed track on the choice of reference frame: Circles calculated for a fixed Iceland hotspot in a fixed-hotspot reference frame (Müller et al., 1993) indicate that the Iceland plume was beneath western Greenland around 60 Ma (Lawver and Müller, 1994). In contrast, the computed positions with a moving Iceland hotspot in a moving-hotspot reference frame (Steinberger et al., 2004) are much closer to the spreading ridge and the Faroe–Iceland ridge before

≈30 Ma. Differences between circles and squares are due to both the computed motion of the Iceland hotspot (squares in Fig. 5) and the difference between the two reference frames.

These plate motion models – both for fixed and moving hotspots – have a lithospheric net rotation, which is interpreted as a net rotation of the mean lithosphere relative to the deep mantle. Such a net rotation may be caused due to lateral viscosity variations within and beneath the lithosphere. For example, a large Pacific plate that is pulled westward by the attached slab may cause an average "westward drift" of the lithosphere. In the numerical flow model, which does not consider lateral viscosity variations, any lithospheric net rotation has to be introduced artificially.

In the results so far, this has been done by computing flow in the mantle and hotspot motion in a "no-net-rotation reference frame" but computing hotspot tracks with lithospheric plate motions in a frame with net rotation (Fig. 6, bottom right). In model 2 e, though, the whole mantle has the same net rotation as the lithosphere (Fig. 6, bottom left). In the vicinity of Iceland this introduces an additional uniform southwestward flow component of about 1 cm/yr, and hence corresponding hotspot motion (model 2 e). Without a self-consistent model explaining lithospheric net rotation relative to the deeper mantle it remains difficult to assess how much of the relative net rotation, which is artificially introduced in model 2 a, is real in the vicinity of Iceland. In favour of the relative net rotation, results in model 2 a appear more realistic than in model 2 e, in that the computed past plume location is closer to the Faroe–Iceland ridge.

2.7. Effect of large-scale density model on hotspot motion

Fig. 8 shows computed tracks for the three different tomography models (2 b, 2 c, 2 d) that were used to construct the smean model, for which results are shown in Figs. 5 and 7. Since tracks were all computed in the same reference frame, differences shown here indicate differences in computed hotspot motion resulting from different global mantle flow fields: All yield about 300 km westward motion as shown for smean in Fig. 5, but the TXBW model additionally gives about 150 km southward motion, the SB4L18 model about the same amount of northward motion.

3. Regional model of Iceland plume and mid-Atlantic ridge

The regional model allows a more quantitative assessment of plume–ridge interaction in order to explain the bathymetry of the North Atlantic. We use the flow velocities of the global model as mechanical boundary conditions of a regional thermo-mechanical model of the North Atlantic upper mantle with temperature and depth dependent viscosity.

3.1. Regional flow computation

Regional flow was computed with a modified version of the code of Albers (2000a). The code solves the conservation equations of mass, momentum and energy using finite volume discretization and multigrid method. The size of the model box is

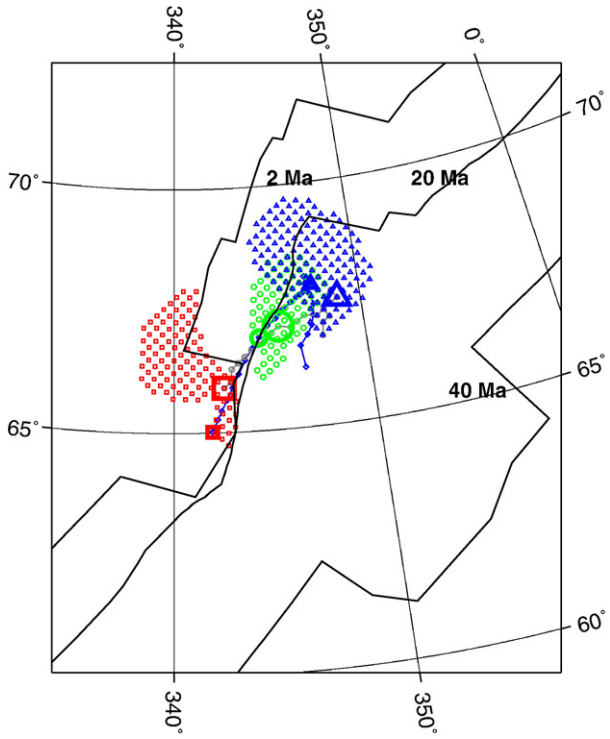

Fig. 9. Comparison of plume motion in the regional model (case 3 a) and global model (case 2 h). Big symbols show the plume conduit position at 200 km depth in the regional model; medium size symbols are for the global model. Small symbols show the regions hotter than 120 K at 100 km depth in the regional model. They are shown at 40 Ma (blue triangles), 20 Ma (green circles) and 2 Ma time (red rectangles). Blue small diamonds connected with a blue line show plume conduit motion at 200 km depth in the global model between 60 Ma and 0 Ma.

$96 \cdot 96 \cdot 32$ grid cells, corresponding to $1980\,\text{km} \cdot 1980\,\text{km} \cdot 660\,\text{km}$ (Fig. 3). Local grid refinements are introduced in the regions of high viscosity contrast. The temperature difference between the bottom and the top of the model box is 1300 K. The initial temperature profile represents a 100 km thick lithosphere and reflects lithospheric cooling. The initial viscosity structure is shown in Fig. 2. The time-dependent plate motion model explained in Section 2.2. was used on the surface of the model box as boundary condition from 56 Ma. Before 56 Ma, surface motion for the entire box was inferred from the coherent Eurasia–Greenland plate motion. On the sides and bottom of the regional model box, velocities based on the global model were applied as time-dependent boundary conditions.

For a smooth transition between the flow fields V_{NN} in the no-net rotation reference frame used in the deep mantle and V_{HS} in the hotspot reference frame, used in the lithosphere, we take a combined flow field

$$V_{\text{global}} = V_{\text{NN}} \cdot (1 - f(z)) + V_{\text{HS}} \cdot f(z) \tag{1}$$

with

$$f(z) = 0.5 + \frac{1}{\pi} \arctan\left(\alpha(z - d)\right) \tag{2}$$

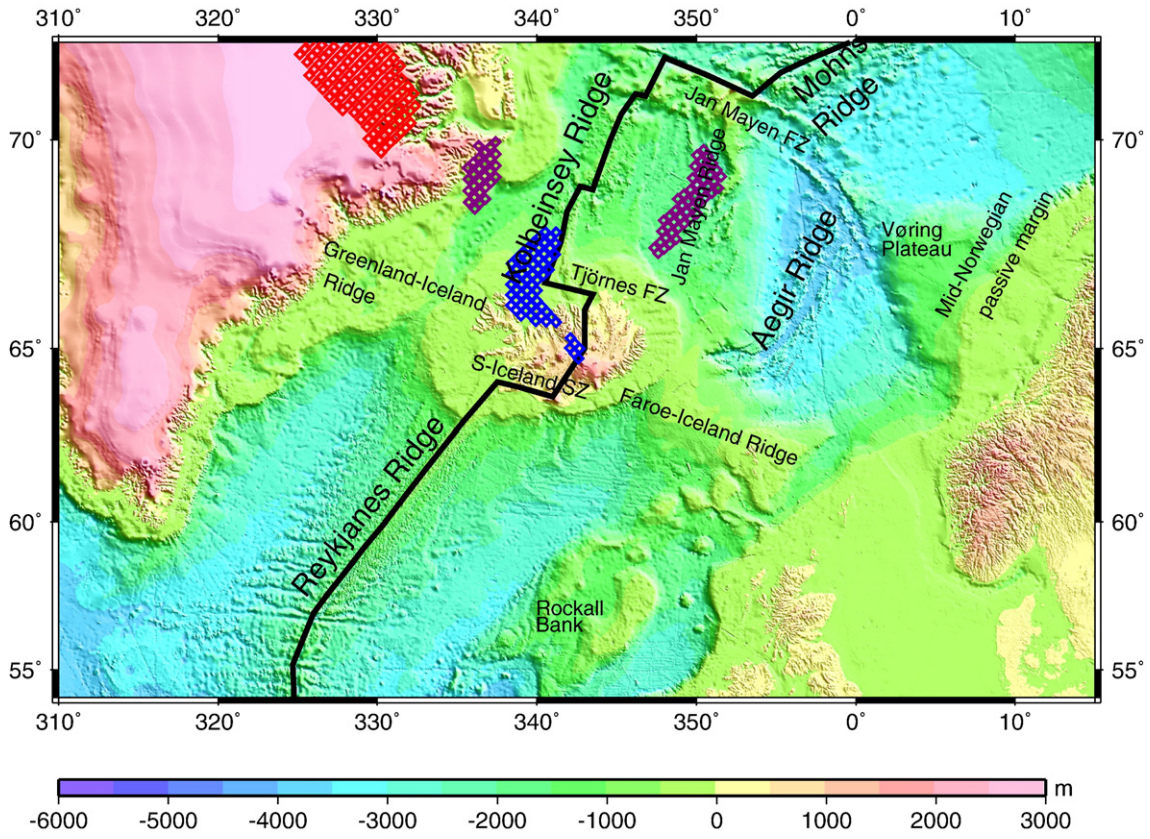

Fig. 10. Model 3 a (moving-source) plume head track for 40 Ma (red diamonds), 20 Ma (purple diamonds), and 0 Ma (blue diamonds), and bathymetry of the North Atlantic.

z is the normalized vertical coordinate ($z=0$ at 660 km, $z=1$ at the surface). The value of d approximately corresponds to the minimum in the viscosity structure, where the transition between the two reference frames is expected. We also find that the average procentual difference between global flow field and regional flow field computed without plume and with boundary conditions from global flow as a function of d has a local minimum of about 12% for $d=0.7$. The grid on which the global mantle flow field was calculated is equidistant longitudinally with a grid spacing of 5.625°; latitudinally 32 Gaussian latitudes were used. If this grid structure is refined laterally, the calculated global mantle flow field does not show more details, due to the resolution limit of the tomography models used. However, if the vertical resolution of the grid is increased above the resolution of the tomography model, the resulting flow field shows more details under the lithosphere, where the viscosity has its minimum. We found that an adequate resolution is obtained if the flow field is computed on ten equidistant layers in the upper mantle.

The plume is introduced by adding a temperature anomaly of 200 K shaped as a Gaussian function centered on the position of the plume at the bottom of the model box. Vertical velocity was also increased at the location of the plume in a way that an anomalous mass flux was set to 1200 kg/s. The computation is started at 60 Ma such that the plume arrives below the lithosphere at ≈50 Ma, corresponding to a rise time of ≈10 Ma through the upper 660 km. In case 3 b, the plume position was fixed, in case 3 a it was taken from global model case 2 h. The extra material influx due to the plume was balanced by an extra outflux distributed over the four sides of the model box. To compensate for introducing the plume explicitly, density anomalies within the regional model box were excluded here (in model cases 3 only) when calculating the global flow field.

3.2. Conduit motion and hotspot tracks in the regional flow model

The main new effect added by the regional model is that motion of the plume is now influenced also by lateral viscosity variations corresponding to lithospheric thickness variations in the vicinity of the ridge.

3.2.1. Conduit motion

The motion of the plume was calculated in the time interval between 60 Ma and present-day in the regional model (Fig. 9). At 40 Ma the plume is in an off-ridge position. The plume head (by which we mean the region hotter than 120 K at 100 km depth) is slightly elongated in a northwest–southeast direction and not centered on the plume conduit position but shifted to the northwest due to the large-scale mantle flow below the lithosphere. The ridge is situated about 300 km southeast of the plume head and no plume–ridge interaction develops, because the asthenospheric flow pushes the plume head away from the ridge. Interaction of the plume with the ridge develops at about 36 Ma shortly before

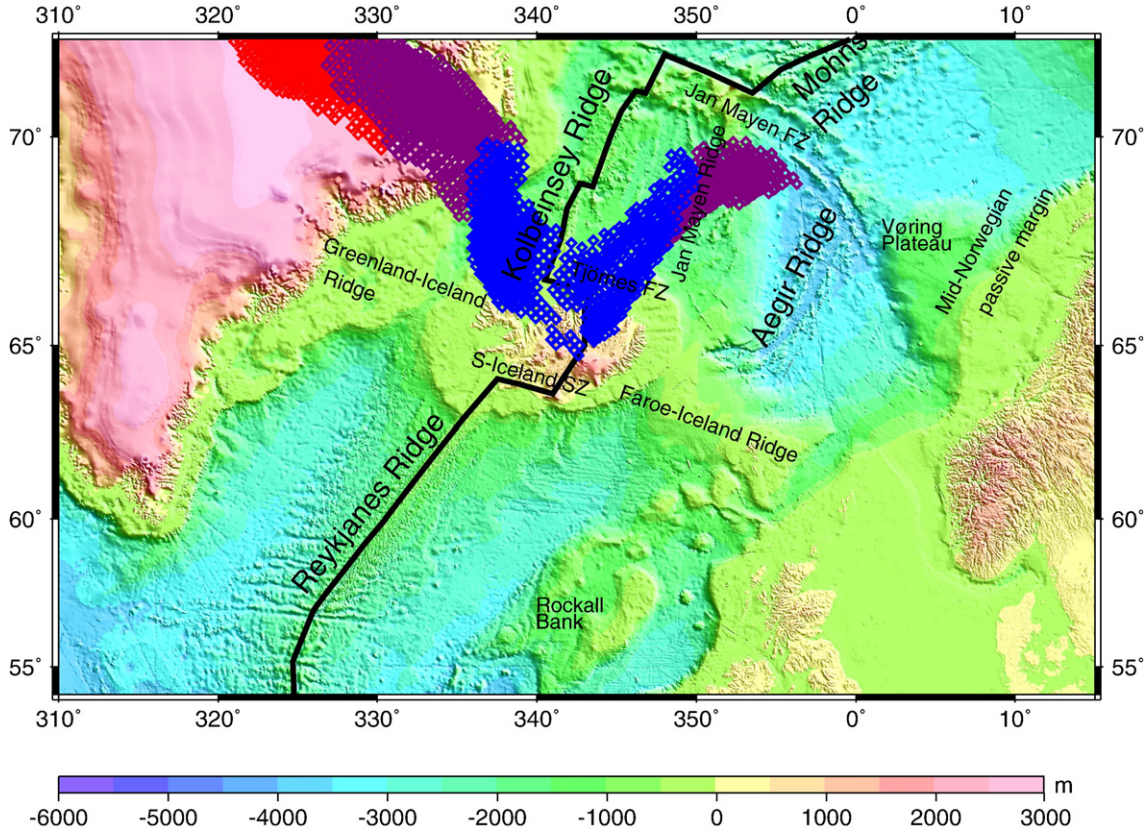

Fig. 11. Model 3 a (moving source) plume head track for 50 Ma–40 Ma (red diamonds), 40 Ma–20 Ma (purple diamonds), and 20 Ma–0 Ma (blue diamonds), and bathymetry of the North Atlantic.

the ridge jump (http://www.geophysik.uni-frankfurt.de/sagert/). After the ridge jump at 32 Ma the new ridge is formed above the center of the plume head. At 20 Ma the plume is ridge-centered and the plume head is elongated along the ridge and shifted to the north relative to the plume conduit. At 2 Ma the plume head is situated north of the plume conduit and extends to the north beyond Tjörnes fracture zone following the shape of the ridge. The plume conduit position below the plume head calculated in the global and regional model (2 h and 3 a) slightly differs, due to the different geometry of the two models and the difference in buoyancy fields.

3.2.2. Plume head tracks

In order to investigate in what way the inclusion of the plume–ridge interaction changes the calculated hotspot track we have calculated plume head tracks by combining the area of the plume head with the plate motion model. In contrast to the models 2 tracks represented by a chain of points (Figs. 7 and 8) the calculated plume head track is a 200–300 km wide strip (Figs. 10 and 11). The 2 h hotspot track is situated inside the 3 a plume head track, since the surface projection of the plume conduit is situated always inside the plume head (Fig. 9). Thus the 3 a plume head track follows the same curvature as the 2 h hotspot track, but it is wider. The 3 a track on the European side partly falls on the Jan Mayen ridge and covers an area offshore Iceland with no thickened crust (Fig. 11). On the American side the track is to the north of the Greenland–Iceland ridge.

The model 3 b track, computed for a fixed plume location at 660 km depth, is more straight than the model 3 a track (Figs. 12 and 13). On the American side the 3 b track fits better the Greenland–Iceland track. On the European side the track fits approximately the shelf of Iceland (Fig. 13). The asymmetry in the extent of the track on the European and American plates is due to the fact, that the plume was initially under the Greenland plate on the American side. Plume–ridge interaction starting earlier would produce tracks which are more symmetric over the plates.

4. Discussion

The assumption that the plume conduit is advected in the large-scale mantle flow field results generally in a computed westward motion of the plume, with variable amounts of southward motion, depending on modeling assumptions. Combination of models of plume motion and plate motion allows us to predict hotspot tracks and compare their location with regions of thickened oceanic crust, formed presumably under the influence of the plume.

In general, more southerly plume and track positions are more suitable to explain the locations where thickened oceanic crust formed. A suitable southerly plume position can be computed

with a variety of modeling assumptions: (A) By assuming the plume source is at depth 660 km and not in the lower mantle; then the plume is not affected by southward mantle flow in the lower mantle (Fig. 4). (B) By assuming the plume reached the surface only about 60 Ma ago, i.e. does not much predate the opening of the Atlantic, and was vertical at that time. Then the lower part of the plume conduit has not moved so much southward, and rising of a tilted conduit does not much contribute to hotspot motion (Fig. 4). (C) By choice of an appropriate density model, within the uncertainties of density models provided by seismic tomography (Fig. 8). Additionally, the choice of reference frame also affects the predicted hotspot track: Considering the net rotation of the lithosphere yields a more suitable, southerly track, and so does a moving-hotspot mantle reference frame, when compared to a fixed-hotspot reference frame (Fig. 7).

With a regional flow computation, the effect of plume–ridge interaction was studied. We found the plume gets affected by the presence of the ridge only 4 Ma prior to getting overridden by the ridge (Fig. 9). Due to large-scale flow, the plume head is shifted northward relative to the plume conduit. The limited material transport to the ridge in the model computation may be due to a number of causes. The sloping base of the lithosphere, which can have an important role in plume–ridge interaction (Kincaid et al., 1996) started to form in the model at 56 Ma time, as the surface velocity field triggered the continental breakup. During the mechanically driven transformation of the thermal structure of a plate to the thermal structure of the ridge, the effect of the sloping base of the lithosphere was reduced. Scale-laws describing steady-state plume–ridge interaction fail to explain the plume–ridge interaction in our model, which is not steady-state. Our results are in accord with the prediction of a less strong plume–ridge interaction when a plume progresses towards a ridge, compared to the case when it progresses away (Ribe and Delattre, 1998). In the case of Iceland, the plume does not progress away from the ridge, but remains close to the ridge after being overridden.

By combining the regional plume model with a plate motion model, we computed plume head tracks. Again, a model with substantial southward plume motion, and/or northward plate motion does not match well the topography high of the straight Greenland–Iceland–Faroe ridge (Figs. 10 and 11). Figs. 12 and 13 show a result that fits better the straight Greenland–Iceland part of the Greenland–Iceland–Faroe ridge. The track at 20 Ma fits the continental shelf of Iceland. However, the Faroe plateau is not explained by the calculated plume head track. This example was calculated for a fixed plume source, but similar results could presumably be achieved with a model of plume motion that is mostly westward and less southward, or by combining with plate motions in the moving-hotspot mantle reference frame, which gives smaller northward plate motion components in the vicinity of Iceland compared to the fixed-hotspot reference frame. A westward moving plume source at depth 660 km, as

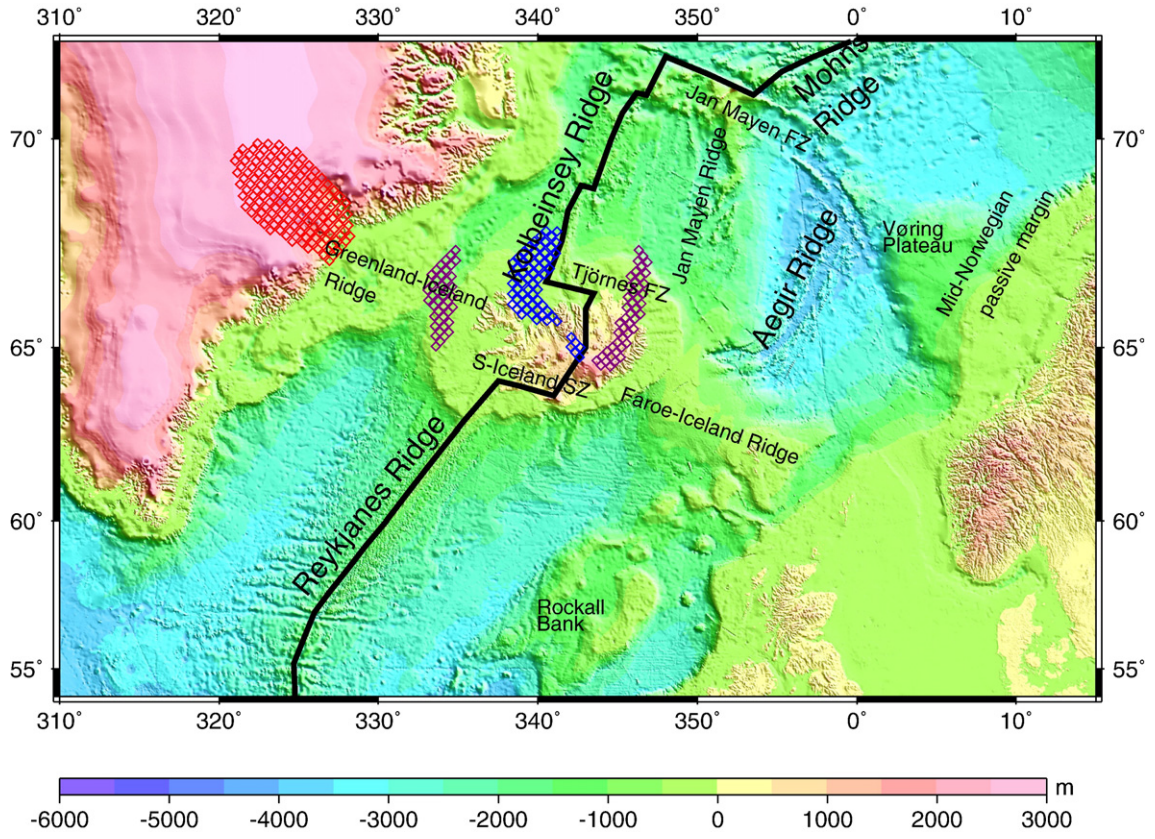

Fig. 12. Model 3 b (fixed source) plume head track for 40 Ma (red diamonds), 20 Ma (purple diamonds), and 0 Ma (blue diamonds) and bathymetry of the North Atlantic.

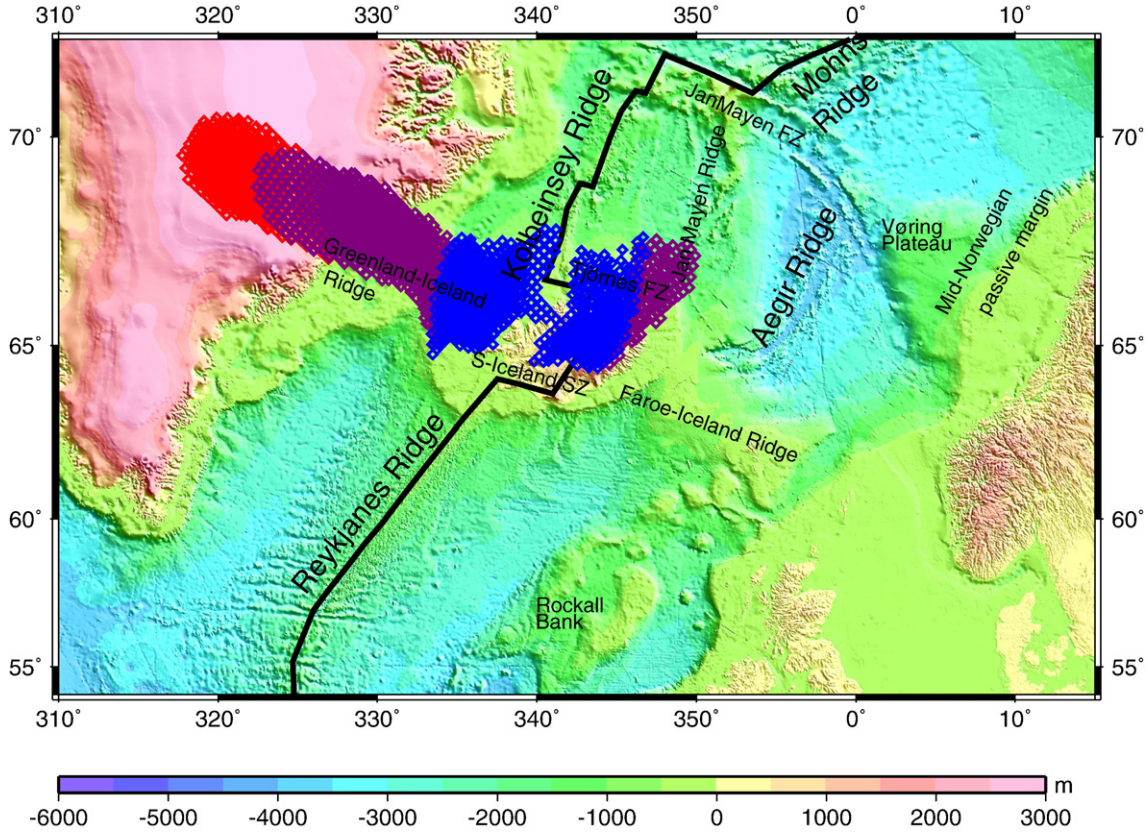

Fig. 13. Model 3 b (fixed source) plume head track for 50 Ma–40 Ma (red diamonds), 40 Ma–20 Ma (purple diamonds), and 20 Ma–0 Ma (blue diamonds) and bathymetry of the North Atlantic.

in models 2 a and 2 g, would presumably yield an earlier start of plume–ridge interaction and the model track could presumably fit the Faroe plateau better.

5. Conclusion

The dynamic models of the large-scale mantle flow field show little variation due to the uncertainties of tomography models. The configuration of the ridge and the Iceland plume and the direction of the large-scale mantle flow field in the North Atlantic do not enhance plume–ridge interaction in the 60 Ma–30 Ma time interval. For a whole-mantle plume our model often predicts a substantial southward component of hotspot motion, which makes it more difficult to explain the Faroe–Iceland ridge as a feature caused by the Iceland plume. An upper-mantle plume model yields a westward motion which is more consistent with the bathymetry of the North Atlantic. This may indicate that the Iceland plume is restricted to the upper mantle. However, some models for lower-mantle plumes yield very similar results, such that currently results remain inconclusive regarding the question of depth of plume origin.

Acknowledgments

The refinement of the plate boundary model in the North Atlantic was Irina Sagert's work. Thanks to Gabriele Marquart for information on bathymetry data. Funding was provided by the Deutsche Forschungsgemeinschaft, Project Number STE 907/6-1. B.S. acknowledges funding through a visiting fellowship at the Cooperative Institute for Research in Environmental Sciences (CIRES). P.M. acknowledges funding of the Hungarian grant OTKA T037980. Figures were prepared using GMT (Wessel and Smith, 1998).

References

Albers, M., 2000a. A local mesh refinement multigrid method for 3-D convection problems with strongly variable viscosity. J. Comp. Phys. 160, 126–150.

Albers, M., 2000b. Numerische Untersuchungen zur Wechselwirkung von Mantelplumes mit Mittelozeanisches Rücken. Ph.D. thesis, Universit ät Göttingen (in german).

Anderson, D., 2000. The thermal state of the upper mantle; no role for mantle plumes. Geophys. Res. Lett. 27, 3623–3626.

Becker, T.W., Boschi, L., 2002. A comparison of tomographic and geodynamic mantle models. Geochem. Geophys. Geosys. 3 (2000GC000168).

Bijwaard, H., Spakman, W., 1999. Tomographic evidence for a narrow whole mantle plume below Iceland. Earth Planet. Sci. Lett. 166, 121–126.

Bjarnason, I.T., Silver, P.G., Rümpker, G., Solomon, S.C., 2002. Shear wave splitting across the Iceland hotspot: results from the ICEMELT experiment. J. Geophys. Res. 107 (B12), 2382. doi:10.1029/JB000916.

Brandsdottir, B., Menke, W., Einarsson, P., White, R.S., Staples, R.K., 1997. Froe–Iceland Ridge experiment 2. Crustal structure of the Krafla central volcano. J. Geophys. Res. 102, 7867–7887.

Bunge, H.-P., Hagelberg, C.R., Travis, B.J., 2003. Mantle circulation models with variational data assimilation: inferring past mantle flow and structure from plate motion histories and seismic tomography. Geophys. J. Int. 152, 280–301.

Čadek, O., Fleitout, L., 2003. Effects of lateral viscosity variations in the top 300 km on geoid, dynamic topography and lithospheric stresses. Geophys. J. Int. 152, 566–580.

Conrad, C.P., Gurnis, M., 2003. Seismic tomography, surface uplift, and the breakup of Gondwanaland: integrating mantle convection backwards in time. Geochem. Geophys. Geosys. 4 (2001GC000299).

Courtillot, V., Davaille, A., Besse, J., Stock, J., 2003. Three distinct types of hotspots in the Earth's mantle. Earth Planet. Sci. Lett. 205, 295–308.

Davaille, A., 1999. Simultaneous generation of hotspots and superswells by convection in a heterogeneous planetary mantle. Earth Planet. Sci. Lett. 402, 756–760.

Evans, J.R., Sacks, I.S., 1979. Deep structure of the Iceland Plateau. J. Geophys. Res. 84, 6859–6865.

Foulger, G.R., Pritchard, M.J., Julian, B.R., Evans, J.R., Allen, R.M., Nolet, G., Morgan, W.J., Bergsson, B.H., Erlendsson, P., Jakobsdottir, S., Ragnarsson, S., Stefansson, R., Vogfjord, K., 2000. The seismic anomaly beneath Iceland extends down to the mantle transition zone and no deeper. Geophys. J. Int. 142, F1–F5.

Gaina, C., Roest, W., Müller, R.D., 2002. Late Cretaceous — Cenozoic deformation of northeast Asia. Earth Planet. Sci. Lett. 197, 273–286.

Gao, S., Davis, P.M., Liu, H., Slack, P.D., Rigor, A.W., Zorin, Y.A., Mordvinova, V.V., Kozhevnikov, V.M., Logatchev, N.A., 1997. Sks splitting beneath continental rift zones. J. Geophys. Res. 102 (B10), 22781–22798.

Gordon, R.G., Jurdy, D.M., 1986. Cenozoic global plate motions. J. Geophys. Res. 91, 12389–12406.

Grand, S., 2002. Mantle shear-wave tomography and the fate of subducted slabs. Philos. Trans. R. Soc. Lond. Ser A: Math. Phys. Sci. 360, 2475–2491.

Hager, B.H., O'Connell, R.J., 1979. Kinematic models of large-scale flow in the Earth's mantle. J. Geophys. Res. 84, 1031–1048.

Hager, B.H., O'Connell, R.J., 1981. A simple global model of plate dynamics and the mantle convection. J. Geophys. Res. 86, 4843–4867.

Ito, G., Lin, J., Graham, D., 2003. Observational and theoretical studies of the dynamics of mantle plume-mid-ocean ridge. Rev. Geophys. 41 (4), 1017. doi:10.1029/2002RG000117.

Jellinek, A.M., Gonnermann, H.M., Richards, M.A., 2003. Plume capture by divergent plate motions: implications for the distribution of hotspots, geochemistry of mid-ocean ridge basalts, and estimates of the heat flux at the core-mantle boundary. Earth Planet. Sci. Lett. 205, 361–378.

Kaban, M.K., Flovenz, O.G., Palmason, G., 2002. Nature of the crust–mantle transition zone and the thermal state of the upper mantle beneath Iceland from gravity modelling. Geophys. J. Int. 149, 281–299.

Karato, S., 1993. Importance of anelasticity in the interpretation of seismic tomography. Geophys. Res. Lett. 20, 1623–1626.

Kaus, B.J.P., Podladchikov, Y.Y., 2001. Forward and reverse modeling of the three-dimensional viscous Rayleigh–Taylor instability. Geophys. Res. Lett. 28, 11095–11098.

Kincaid, C., Schilling, J.-G., Gable, C., 1996. The dynamics of off-axis plumeridge interaction in the uppermost mantle. Earth Planet. Sci. Lett. 137, 29–43.

Kodaira, S., Goldschmidt, R., Hartmann, J.M., Hirschleber, H.B., Iwasaki, T., Kanazawa, T., Krahn, H., Tomita, S., Shimamura, H., 1995. Crustal structure of the Lofoten continental margin, off northern Norway, from ocean-bottom seismographic studies. Geophys. J. Int. 121, 907–924.

Kodaira, S., Mjelde, R., Gunnarsson, K., Shiobara, H., Shimamura, H., 1997. Crustal structure of the Kolbeinsey Ridge, North Atlantic, obtained by use of ocean bottom seismographs. J. Geophys. Res. 102, 3131–3151.

Lawver, L.A., Müller, R.D., 1994. Iceland hotspot track. Geology 22, 311–314.

Marquart, G., Schmeling, H., 2004. A dynamic model for the iceland plume and the north atlantic based on tomography and gravity data. Geophys. J. Int. 159, 40–52.

Masters, G., Laske, G., Bolton, H., Dziewonski, A.M., 2000. The relative behavior of shear velocity, bulk sound speed, and compressional velocity in the mantle: implications for chemical and thermal structure. In: Karato, S.-I., Forte, A.M., Liebermann, R.C., Masters, G., Stixrude, L. (Eds.), Earth's Deep Interior: Mineral Physics and Tomography From the Atomic to the Global Scale. Geophys. Monogr. Ser., vol. 117. AGU, Washington D.C., pp. 63–87.

Menke, W., Levin, V., 1994. Cold crust in a hot spot. Geophys. Res. Lett. 21, 1967–1970.

Montelli, R., Nolet, G., Dahlen, F.A., Masters, G., Engdahl, E.R., Hung, S.-H., 2004. Finite-frequency tomography reveals a variety of plumes in the mantle. Science 303, 338–343.

Morgan, W.J., 1971. Convection plumes in the lower mantle. Nature 230, 42–43.

Müller, R., Royer, J.-Y., Lawver, L.A., 1993. Revised plate motions relative to hotspots from combined Atlantic and Indian Ocean hotspot tracks. Geology 21, 275–278.

Müller, R.D., Roest, W.R., Royer, J.-Y., Cahagan, L.M., Sclater, J.C., 1997. Digital isochrons of the world's ocean floor. J. Geophys. Res. 102 (B2), 3211–3214.

Ribe, N.M., Delattre, W.L., 1998. The dynamics of plume–ridge interactions — iii. The effects of ridge migration. Geophys. J. Int. 133, 511–518.

Ritsema, J., van Heijst, H.J., 2000. Seismic imaging of structural heterogeneity in Earth's mantle: evidence for large-scale mantle flow. Sci. Prog. 83, 243–259.

Roest, W.R., Srivastava, S.P., 1989. Seafloor spreading in the Labrador Sea: a new reconstruction. Geology 17, 1000–1004.

Schilling, J.-G., 1991. Fluxes and excess temperatures of mantle plumes inferred from their interaction with migrating mid-oceanic ridges. Nature 352, 397–403.

Shen, Y., Solomon, S.C., Bjarnason, I.T., Nolet, G., Morgan, W.J., Allen, R.M., Vogfjrd, K., Jakubsdottir, S., Stefnsson, R., Julian, B.R., Foulger, G.R., 2002. Seismic evidence for a tilted mantle plume and north–south mantle flow beneath Iceland. Earth Planet. Sci. Lett. 197, 261–272.

Sleep, N.H., 1990. Hotspots and mantle plumes: some phenomenology. J. Geophys. Res. 95, 6715–6736.

Smallwood, J.R., 1999. Crust generated above the Iceland mantle plume: from continental rift to oceanic spreading center. J. Geophys. Res. 104, 22885–22902.

Smith, W.H.F., Sandwell, D.T., 1997. Global seafloor topography from satellite altimetry and ship depth soundings. Science 277, 1957–1962.

Staples, R.K., White, R.S., Bransdottir, B., Menke, W., Maguire, P.K.H., McBridge, J.H., 1997. Faeroe–Iceland Ridge Experiment 1. Crustal structure of northeastern Iceland. J. Geophys. Res. 102, 7849–7866.

Steinberger, B., O'Connell, R., 1998. Advection of plumes in mantle flow: implications for hotspot motion, mantle viscosity and plume distribution. Geophys. J. Int. 132, 412–434.

Steinberger, B., Sutherland, R., O'Connell, R.J., 2004. Prediction of Emperor–Hawaii seamount locations from a revised model of plate motion and mantle flow. Nature 430, 167–173.

Su, W.-J., Dziewonski, A.M., 1997. Simultaneous inversion for 3-D variations in shear and bulk velocity in the mantle. Phys. Earth Planet. Inter. 100, 135–156.

Thorbergsson, G., Magnússon, I.T., Pálmason, G., 1993. Gravity Data and Gravity Map of Iceland. Orkustofnun Íslands. OS-93027/JHD-07.

Vink, G.E., 1984. A hotspot model for Iceland and the Vøring Plateau. J. Geophys. Res. 89, 9949–9959.

Wessel, P., Smith, W.H.F., 1998. New, improved version of the Generic Mapping Tools released. EOS Trans. AGU 79.

White, R.S., 1997. Rift–plume interaction in the North Atlantic. Philos. Trans. R. Soc. Lond. 355, 319–339.

Zhang, S., Christensen, U., 1993. Some effects of lateral viscosity variations on geoid and surface velocities induced by density anomalies in the mantle. Geophys. J. Int. 114, 531–547.